Effects of Ce^{3+} doping on structural, morphological, optical properties of ZnO nanoparticles: Enhanced photo-catalytic and antibacterial activity

S. Gunasekaran[1], S. Shankar[1], G. Padma Priya [2*], V. Thirumurugan[1]

[1] P.G and Research Department of Chemistry, A.V.V.M Sri Pushpam College, Poondi, Thanjavur - 613503, Tamil Nadu, India

[2] Department of Chemistry, Bharath Institute of Higher education and Research (BIHER), Bharath University, Chennai–600073, Tamil Nadu (TN)

*** Corresponding author: Email: prwwwprcom47@gmail.com**

Abstract

Different concentration of cerium doped zinc oxide ($Ce_xZn_{1-x}O$ $0.0 \leq x \leq 0.07$) nanoparticles (NPs) were synthesized via co-precipitation method using zinc acetate, cerium nitrate as precursors, octylamine as capping and reducing agent. The structures, morphologies, optical activity (photoluminescence) and antibacterial properties of $Ce_xZn_{1-x}O$ were analyzed by Fourier transform infrared (FT-IR) spectroscopy, X-ray powder diffraction (XRD), High resolution scanning electron microscopy (HR-SEM), Energy dispersive X-ray (EDX), High resolution transmission electron microscopy (HR-TEM), UV-Visible, Photoluminescence (PL) spectroscopy. The antibacterial activities of $Ce_xZn_{1-x}O$ NPs were tested by modified Disc diffusion method. The XRD results showed that the Ce^{3+} ions were successfully incorporated into the ZnO host, and the products were well-crystalline nature. The average crystallite size of

$Ce_xZn_{1-x}O$ ($0.0 \leq x \leq 0.07$) NPs were found to be in the range 15.64 nm -12.33 nm. In addition, the sphere-like morphology of $Ce_xZn_{1-x}O$ NPs was confirmed by HR-SEM and HR-TEM images. The band gap of products was varying with the cerium substitution (x) and it increases the defects in ZnO and hence resulting red shift in UV emission which indicate the presence of narrow band gap in the products. In addition the as-synthesized $Ce_xZn_{1-x}O$ NPs have important antibacterial activity against *P.mirabilis, S.typhi*.

Keywords: Nanomaterials; Optical properties; ZnO; TEM; Antibacterial activity.

1. Introduction

The metal oxides with nanostructure possess certain unique properties like optical, phototocatalytic activity, semiconducting, insulating behavior etc., over their same bulk materials [1-3]. Particularly, the zinc oxide (ZnO) NPs has attracted researchers on account of its high photocatalytic activity, low-cost, easy fabrication, unique optical, magnetic and electronic properties etc. [4-9]. ZnO NPs has band gap energy of 3.37eV and great excitation binding energy of 60 meV at room temperature and it also showed excellent ultraviolet absorbance and antibacterial activity. Optical measurements confirmed the potential usage of ZnO NPs as translucent piezo electric and electro conductive materials. Several methods have been adopted for the synthesis of ZnO NPs which include hydrothermal, sol-gel, chemical precipitation, and microwave irradiation methods resulting different structures like nanoflakes, nanowires, nanoflowers and nanorods. The optical, magnetic and catalytic properties of ZnO NPs can be altered by doping with different types of metallic ions [10-12]. The doped ZnO NPs are acted as photocatalysts, gas sensors, light-emitting materials, solar cells, field-effect transistors, biological

systems (bio-imaging, drug delivery, etc.) and as a base material for magnetic semiconductor. In addition, doping of ZnO NPs with rare earth elements (like Ce, La, Tb, Er, Eu, Dy and Sm) shows certain interesting properties like efficient modulation of the emission in the visible range.

Current work is focused on investigating the result of cerium doping concentration on the structure, morphological and optical properties of ZnO NPs prepared by a facile chemical precipitation method using zinc acetate as source of Zn^{2+} ions and cerium nitrate as source of Ce^{3+}ions. The chemical precipitation method to synthesis of $Ce_xZn_{1-x}O$ NPs has many advantages like high quality, low-processing cost, quite low temperature and higher yield etc. over other methods.

2. Materials and Methods

2.1. Chemicals

Zinc acetate ($Zn(Ac)_2$), Cerium nitrate ($Ce(NO_3)_3.6H_2O$), Octylamine ($C_8H_{19}N$), methanol (CH_3OH) were purchased from Sigma-Aldrich and used without further purification.

2.2. Synthesis of $Ce_xZn_{1-x}O$ ($0.0 \leq x \leq 0.07$) NPs

Both ZnO and $Ce_xZn_{1-x}O$ ($0.0 \leq x \leq 0.07$) NPs were prepared by co-precipitation method using zinc acetate, cerium nitrate as metal precursors (Zn, Ce respectively) and octylamine as reducing and capping agent. The solution of 0.1M of zinc acetate in 100 mL methanol was added with 1 mL of octylamine then stirred vigorously for 24h t RT to obtain homogenous precursor solution. To this precursor solution, different moles (0.03, 0.05, 0.07) of $Ce(NO_3)_3$ were added and stirred continuously for 3h. Later 3 M NaOH was added drop wise into the obtained solution until pH attains 12. The resulting solution was aged for 1h and the precipitates were collected and washed using distilled water to remove the unreacted reagents. The slurry was dried in an

oven at 80˚C for about 10h and annealed at 400˚C for 2h. The pure ZnO NPs was prepared by adopting the same procedure without the addition of $Ce(NO_3)_3$.

2.3. Characterization

X-ray powder diffraction (XRD) pattern was recorded using PAN analytical X′Pert PRO equipment using CuK_α (λ = 1.5418 Å). The morphology and elemental composition analysis of the samples were investigated by High resolution scanning electron microscope using (JEOL, JSM-67001). The optical absorption spectra were recorded by UV-Vis absorption spectrometer (Perkin Elmer T90 Spectrophotometer). Room-temperature photoluminescence spectral measurements were carried out using JY Fluorolog 3-11 spectrometer. The solid phase FT-IR spectrum in KBr pellet technique was recorded with (FT-IR; JASCO, Model 6300).

2.4 Photocatalytic activity

The Photocatalytic activities were performed using Methylene Blue (MB) textile dye in the solution under solar light. The average intensity of sunlight signal the surface of the reaction solution was about 90,000 lux, as measured by a digital lux meter. To demonstrate the potential applicability of pure ZnO and Ce doped ZnO NPs in environmental remediation, its photocatalytic activity was carried out in deionized water. The photocatalytic experiments were carried out with 100 mL solutions of MB (5 X 10^{-5} M) and 10 mg of the catalyst under constant stirring. About 3 mL of the aliquot solution was withdrawn at the different time interval (for every 20 min) from the reaction mixture was measured by UV-Vis Spectrophotometer. The photocatalytic degradation can be evaluated by measuring the absorbance of MB solution at 653 nm.

2.5. Antibacterial activity

Antimicrobial activity of the prepared samples was tested in both gram-negative and gram-positive bacteria namely *Staphylococcus aureus*, *Proteus mirabilis*, S*almonella typhii* and *Bacillus subtilis* by disc diffusion method with small modifications. The 24h bacterial cultures were swabbed in a Muller Hinton agar amended plates. Whatmann filter paper discs of 3 mm diameter were impregnated with 100 μL of the solution containing $Ce_xZn_{1-x}O$ ($0.0 \leq x \leq 0.07$ NPs and these discs could evaporation for 1 h. Reference standard discs were prepared with ampicillin (10 μg/mL) to compare the antibacterial activity of the samples. After drying, the discs were placed in swabbed bacterial plates and incubated at 28 °C for 24h. After incubation, plates were examined for clear zone around the discs. A clear zone more than 2 mm in diameter was taken for antibacterial activity.

3. Results and discussion

3.1. XRD analysis

Figure 1 showed the powder XRD powder patterns of $Ce_xZn_{1-x}O$ ($0.0 \leq x \leq 0.07$) NPs respectively. The diffraction peaks and their relative intensities of $Ce_xZn_{1-x}O$ ($0.0 \leq x \leq 0.07$) NPs were match well with those given by JCPDS card no. 31-1451 of ZnO which indicated that all the samples had typical hexagonal wurtzite structure. In addition, no diffraction peaks of Ce or other impurity phases were found, hence we assume that the Ce ions have evenly substituted into the Zn^{2+} sites or interstitial sites in the ZnO lattice [13]. Furthermore, in Figure 2, the most intense peak of doped ZnO NPs shifted towards higher θ value as a result of the internal strain developed by the substitution of Zn^{2+} (host ions) by Ce dopant [14-16]. The high peak intensity of all peaks suggested that the material was in highly crystalline nature.

The lattice parameter was calculated using the formula given in Eq. (1):

$$\sin^2\theta = \frac{\lambda^2}{4}\left[\frac{4}{3}\left(\frac{h^2+hk+k^2}{a^2}\right)+\frac{l^2}{c^2}\right] \qquad \text{---- (1)}$$

where θ is the diffraction angle, λ, the incident wavelength (λ = 0.1540 nm), *h*, *k*, and *l* are Miller's indices. The obtained lattice parameter values of both undoped and Ce doped ZnO were compiled in Table 1. The calculated lattice parameters of ZnO NPs (x=0.0) is a = 3.251, c = 5.211 and the values are increased with increasing the concentration of Ce-dopant. The results indicated that Ce ions have been incorporated into the ZnO lattice since the ionic radius of Ce^{3+} (1.034 Å) is much bigger than that of Zn^{2+} (0.74 Å). Similar result was reported by Aisah et al. [17]. In addition, *c/a* of $Ce_xZn_{1-x}O$ ($0.0 \leq x \leq 0.07$) NPs are 1.603, 1.601, 1.600, 1.598, respectively, was almost constant and has good correlation with the standard value (1.60). The results indicated that the incorporation of Ce ion in the ZnO matrix has no or little effect in the entire crystal structure of host compound.

The average crystallite size was calculated using Scherer formula given in Eq. (2):

$$L = \frac{0.89\lambda}{\beta\cos\theta} \qquad \text{---- (2)}$$

where *L* is the crystallite size, λ, the X-ray wavelength, θ, the Bragg diffraction angle and β, the full width at half maximum (FWHM). The average crystallite sizes of $Ce_xZn_{1-x}O$ ($0.0 \leq x \leq 0.07$) NPs were given in Table 1. The average crystallite sizes of both ZnO and $Ce_xZn_{1-x}O$ ($0.0 \leq x \leq 0.07$) NPs were found to be 15.64 (ZnO), 14.55 ($Ce_{0.03}Zn_{0.97}O$), 13.46 ($Ce_{0.05}Zn_{0.95}O$) and 12.33 nm ($Ce_{0.07}Zn_{0.93}O$) respectively. Thus, the particle size decreases as a result of Ce doping in ZnO nanostructures. This reduction in the crystallite size is due to distortion in the ZnO matrix by Ce^{3+} dopant ions, which decreases the rate of growth of ZnO.

3.2. FT-IR Analysis

The FT-IR spectra of $Ce_xZn_{1-x}O$ ($0.0 \leq x \leq 0.07$) NPs were shown in Figure 2. The peaks appeared at 718 and 457 cm^{-1} can be attributed to the metal oxygen (Ce-O and Zn-O) bonds. The stretching mode of C–O is observed at 1380 cm^{-1}. A broad band occurred at 3442 and 1620 cm^{-1} attributed to the stretching and bending mode of O–H group in water. The peaks corresponding to Zn-O bonds shifted towards lower wavelength for $Ce_xZn_{1-x}O$ ($0.0 \leq x \leq 0.07$) NPs indicating the incorporation of Ce ions. It was noted from the FT-IR data that the Zn–O vibrational mode was more prominently observed and this clearly concludes a strong doping exist in ZnO NPs.

3.3. Morphological analysis

3.3.1. HR-SEM studies

Figure 3 showed surface morphology of $Ce_xZn_{1-x}O$ ($0.0 \leq x \leq 0.07$) NPs examined by HR-SEM analysis. HR-SEM images clearly indicated the sphere-like morphology of nanoparticles. Furthermore, the size of the microspheres also shows an obvious decrease after Ce doping, as shown in Figure 3. It may be due to the formation of Ce−O−Zn on the surface of Ce-doped microspheres, which restrained the growth of crystalline. In addition, HR-SEM showed a transition from loosely aligned nano-spheres of pure ZnO to tightly aligned nano-spheres (like Cauliflower structure) after the Ce-doping.

3.3.2. HR-TEM studies

The formation of sphere like appearance of $Ce_{0.05}Zn_{0.95}O$ NPs was further confirmed by HR-TEM analysis and shown in Figure 4a. From the TEM results, spherical shaped nanoparticles like morphology of samples were confirmed with the average particle size below 20 nm. Figure 4b shows the corresponding selected area electron diffraction (SAED) pattern of the samples, which clearly showed the highly crystalline nature of the final products. The

chemical purity and elemental composition of the products were analyzed by Energy Dispersive X-ray analysis (EDX) as shown in Figure 4c and d. The EDX results showed the presence of Zn, O and Ce by the presence of their corresponding peaks without any other characteristic peaks and suggested that the prepared sample do not contain any other element impurities.

3.4. Optical properties

The effect of doping concentrations on optical properties of $Ce_xZn_{1-x}O$ ($0.0 \leq x \leq 0.07$) NPs were investigated by UV–Vis diffused reflectance spectra and shown in Figure 5. The optical band gap of Eg is calculated using the following Eq 3 [18, 19],

$$\alpha = A(h\nu - E_g)^n/h\nu \qquad \text{---------- (3)}$$

where A and n is a constant, equal to 1/2 for the direct band gap semiconductor. The band gap of the undoped Ce doped ZnO NPs can be given by plotting the value of $(\alpha h\nu)^2$ against the photon energy ($h\nu$) and the intercept of this linear internal of the energy axis at $(\alpha h\nu)^2$ equal to zero gives the band gap (Figure 5) and listed in Table 1. It was observed that the cerium doping concentration had considerable effects on the band gaps of synthesized $Ce_xZn_{1-x}O$ ($0.0 \leq x \leq 0.07$) NPs. The optical energy band gap (E_g) is decreased from 3.02 to 2.71eV, while varying cerium dopant concentration from 0 to 0.07M. Furthermore, once a Zn site in ZnO was occupied by a Ce dopant, two primary effects were observed: (1) The impurity bands nearer to the lower edge of the conduction band was generated by substituted Ce and (2) The band gap get thin, due to the strong orbital coupling between Ce and O. Hence, the band gap of the synthesized the $Ce_xZn_{1-x}O$ NPs can be tuned by Ce dopant concentration. In addition, the existence of extended UV spectra of the $Ce_xZn_{1-x}O$ ($0.0 \leq x \leq 0.07$) NPs showed its optical capability almost in the whole range of visible light spectra. The broad absorption in visible light range was may be due to the sp–d exchange interactions between the conduction band electrons and the localized d

electrons of the Ce^{3+} ions [20]. Furthermore, the s–d and p–d exchange interactions results a negative and a positive correction to the conduction band and the valence band edges independently, hence strong visible light absorption of the $Ce_xZn_{1-x}O$ ($0.0 \leq x \leq 0.07$) NPs were attained [21, 22]. Consequently, the rare earth (Ce) doping in ZnO matrix expands its visible light response by introducing the impurity energy levels in band gap, which is favorable for several potential applications.

3.5. Photoluminescence (PL) spectral analysis

Figure 6 shows the PL spectra of pure and Ce-doped samples at room temperature. All the samples exhibited UV and blue emission. The strong UV peak corresponds to the near-band-edge emission (NBE) at 395 nm, resulting from the recombination intensities of UV emission peaks can be attributed to the increase of the defects and decrease in the size of ZnO [25]. In addition, the green emissions in ZnO crystal and the transitions involved in zinc interstitials [23]. In Figure 6, it was noted that the UV emission peaks for the $Ce_xZn_{1-x}O$ ($0.0 \leq x \leq 0.07$) NPs exhibit slight red shift while the intensities of free excitons. The enhanced blue emission peaks at 425, 432, 459 and 486 nm were attributed to the defects like oxygen vacancies are severely suppressed. This shift may be due to the band gap narrowing caused by the downshift of the conduction band edge after merging with Ce-related impurity band formed below the conduction band [24]. Decrease in centered 425 nm was also observed. The peak at 504 and 525 nm was due to the radiative recombination of a photogenerated band with an electron occupying the deep oxygen vacancy [26-29]

3.6 Photocatalytic degradation of Methylene Blue (MB)

Photocatalytic activity and the degradation efficiency of pure and Ce doped ZnO nanoparticles was evaluated using MB degradation under solar light irradiation (Figure 7).

Generally, photocatalytic degradation (PCD) is expected to absorb the generation of electron-hole (e^-/ h^+) pairs. When the photocatalyst is irradiated with a photon of energy which equal to or higher than its band gap of the ZnO nanoparticles (e^-/ h^+) is created. Holes can react with water adhering to the surfaces of ZnO NPs to form highly reactive hydroxyl radicals ($OH^\bullet$). Meanwhile, the photo- generated electrons react with oxygen to produce superoxide ($O_2^{\bullet-}$). These e^-/ h^+ pairs get repositioned to the surface of the photocatalyst and interact with the dye molecule to participate in redox reactions and as a result, the dye molecule degrades. The super oxide anion radicals can react with H_2O to form H_2O_2, which could further yield reactive hydroxyl radicals ($OH^\bullet$). These reactive radicals work together and decompose organic compounds into CO_2, H_2O and other minerals [30-33].

3.7. Antibacterial Activities

The antibacterial activities of synthesized $Ce_xZn_{1-x}O$ ($0.0 \leq x \leq 0.07$) NPs were tested against the human pathogens like *Staphylococcus aureus*, *Proteus mirabilis*, S*almonella typhii* and *Bacillus subtilis* with reference to Ampicillin [34-37]. The inhibition zones were shown in Figure 8 and the values are listed in Table 2. From the results, it was observed that the synthesized $Ce_xZn_{1-x}O$ NPs showed desired activity against *P. mirabilis and S. typhi which causes* causes kidney stone and typhoid fever respectively [. 38]The undoped and doped ZnO with low Ce dopant concentration showed no activity against *S. aureus and B. subtilis.* Hence, the synthesized $Ce_xZn_{1-x}O$ ($0.0 \leq x \leq 0.07$) NPs can be used in the treatment of kidney stone and Typhoid Fever.

4. Conclusions

$Ce_xZn_{1-x}O$ ($0.0 \leq x \leq 0.07$) NPs have been synthesized by chemical precipitation route. The XRD measurements confirmed that the particle size (15.64 -12.33nm) of the synthesized

$Ce_xZn_{1-x}O$ NPs decreases with increasing Ce concentrations and possess hexagaonal wurtzite structure. Furthermore, the sphere-like morphology was showed by HR-SEM and HR-TEM analysis. Additionally, the elemental composition was confirmed by EDX analysis. Moreover, it was observed that Ce^{3+} ions were successfully incorporated into the ZnO lattice, and the red shift was appeared in PL spectra for doped nanoparticles compared with undoped one. The band gap energies of doped nanoparticles were decreased from 3.02 to 2.71 eV with increasing the cerium doping concentration. Hence, these results indicated that the cerium doping concentration plays an important role in tuning the size, band gap and PL property of the nanoparticles. In addition the synthesized $Ce_xZn_{1-x}O$ NPs possess significant antibacterial activity against *P.mirabilis, S.typhi* and used for treatment of kidney stone and typhoid fever.

References

[1] R. Kumar, Ahmad Umar, G. Kumar, M. S. Akhtar, Yao Wang, S. H. Kim, *Ce*-doped *ZnO* nanoparticles for efficient photocatalytic degradation of direct red-23 dye, Ceram. Int., 41, 7773-7782 **(2015).**

[2] J. Lang, J. Wang, Q. Zhang, X. Li, Q. Han, M. Wei, Y. Sui, D. Wang, J. Yang, Chemical precipitation synthesis and significant enhancement in photocatalytic activity of Ce-doped ZnO nanoparticles, Ceram. Int., 42, 14175-14181 **(2016).**

[3] N. Sinha, G. Ray, S. Bhandari, S. Godara, B. Kumar, Synthesis and enhanced properties of cerium doped ZnO nanorods, Ceram. Int., 40, 12337-12342 **(2014).**

[4] E. Manikandan, M. K. Moodley, S. S. Ray, B. K. Panigrahi, R. Krishnan, K.G.M. Nair, A. K. Tyagi, Zinc oxide epitaxial thin-film deposited over carbon on various substrates by PLD technique, J. Nanosci. Nanotech. 10, 5601-5611 **(2010).**

[5] J. F.Zhu, Y.J.Zhu, Microwave-assisted one-step synthesis of polyacrylamide-metal (M = Ag, Pt, Cu) nanocomposites in ethylene glycol, J. Phys. Chem. B 110, 8593-8597 **(2006).**

[6] A. Manikandan, E. Manikandan, B. Meenatchi, S. Vadivel, S.K. Jaganathan, R. Ladchumananandasivam, M. Henini, M. Maaza, J.S. Aanand, Rare earth element Lanthanum doped zinc oxide (La: ZnO) nanoparticles: Synthesis structural optical and antibacterial studies, J. Alloys Compd. 723, 1155-1161 **(2017).**

[7] K. Kaviyarasu, E. Manikandan, J. Kennedy, M. Jayachandran, Quantum confinement and photoluminescence of well-aligned CdO nanofibers by a solvothermal rout, Mater. Lett. 120, 243-245 **(2014).**

[8] F. Fang, J. Futter, A. Markwitz, J. Kennedy, Synthesis of zinc oxide nanorods and their sensing properties, Mater. Sci. Forum 700, 150-153 **(2012).**

[9] J. Kennedy, A. Markwitz, Z. Li, W. Gao, Characterization of ZnO films by ion beam analysis, J. Modern Phys. *B* 20, 4655-4660 **(2006).**

[10] B. Sathyaseelan, E. Manikandan, K. Sivakumar, J. Kennedy, M. Maaza, Enhanced visible photoluminescent and structural properties of ZnO/KIT-6 nanoporous materials for white light emitting diode (w-LED) application, J. Alloys Compds. 651, 479-482 **(2015)**

[11] E. Hema, A. Manikandan, P. Karthika, S.A. Antony, B R. Venkatraman, A novel synthesis of Zn^{2+}-doped $CoFe_2O_4$ spinel nanoparticles: Structural, morphological, opto-magnetic and catalytic properties, J. Supercond. Nov. Magn. 28, 2539–2552 **(2015).**

[12] B. Meenatchi, K.R.N. Deve, A. Manikandan, V. Renuga, V. Sathiyalakshmi, Protic ionic liquid assisted synthesis, structural, optical and magnetic properties of Mn-doped ZnO nanoparticles, Adv. Sci. Eng. Med. 8, 653-659 **(2016).**

[13] J.T. Chen, J. Wang, F. Zhang, G.A. Zhang, Z.G. Wu, P.X. Yan, The effect of La doping concentration on the properties of zinc oxide films prepared by the sol–gel method, J. Cryst. Growth 310, 2627–2632 **(2008).**

[14] A.R. Denton, N.W. Ashcroft, Vegard's law, Phys. Rev. A. 43, 3161–3164 **(1991).**

[15] A.S.H. Hameed, C. Karthikeyan, A.P. Ahamed, N. Thajuddin, N.S. Alharbi, S.A. Alharbi, G. Ravi, *In vitro* antibacterial activity of ZnO and Nd doped ZnO nanoparticles against ESBL producing *Escherichia coli* and *Klebsiella pneumonia* Sci. Rep. 6, 24312 **(2016).**

[16] B. Singh, Z.A. Khan, I. Khan, S. Ghosh, Highly conducting zinc oxide thin films achieved without postgrowth annealing,Appl. Phys. Lett. 97, 241903 **(2010).**

[17] N. Aisah, D. Gustiono, V. Fauzia, I. Sugihartono, R. Nuryadi, Synthesis and enhanced photocatalytic activity of Ce-doped zinc oxide nanorods by hydrothermal, Mater. Sci. Eng. 172, 1-8 **(2017).**

[18] J. Cao, J. Yang, Y. Zhang, L. Yang, D. Wang, M. Wei, Y. Wang, Y. Liu, M. Gao, X. Liu, Growth mechanism and blue shift of Mn^{2+} luminescence for wurtzite ZnS:Mn^{2+} nanowires, J. Phys. D Appl. Phys. 43, 075403 **(2010).**

[19] M. Saif, H. Hafez, A.I. Nabeel, Photo-induced self-cleaning and sterilizing activity of Sm^{3+} doped ZnO nanomaterials, Chemosphere 90, 840-847 **(2013).**

[20] S. Liu, C. Li, Y. Jiaguo, Q. Xiang, Improved visible-light photocatalytic activity of porous carbon self-doped ZnO nanosheet-assembled flowers, Cryst. Eng. Comm. 13, 2533 – 2541 **(2011).**

[21] K. Jayanthi, S. Chawla, A.G. Joshi, Z.H. Khan, R.K. Kotnala, Fabrication of luminescent, magnetic hollow core nanospheres and nanotubes of Cr-doped ZnO by inclusive co-precipitation method, J. Phys. Chem. C 114, 18429-18434 **(2010).**

[22] C. Xu, L. Cao, G. Su, W. Liu, X. Qu, Y. Yu, Preparation, characterization and photocatalytic activity of Co-doped ZnO powders, J. Alloys Compd. 497, 373-376 **(2010).**

[23] H. B. Zeng, G. T. Duan, Y. Li, S. K. Yang, X. X. Xu, W. P Cai, Blue luminescence of ZnO nanoparticles based on non-equilibrium processes: defect origins and emission controls, Adv. Funct. Mater. 20, 561−572 **(2010).**

[24] A. Majid, A. Ali, Red shift of near band edge emission in ceriumim planted GaN, J. Phys. D Appl. Phys. 42, 045412 **(2009).**

[25] H. C. Gong, J. F. Zhong, S. M. Zhou, B. Zhang, Z. H. Li, Z. L. Du, Ce-induced single-crystalline hierarchical zinc oxide nanobrushes, Superlatt. Microstruct. 44, 183−190 (2008).

[26] S. H. Jeong, J. K. Kim, B. T. Lee, Effects of growth conditions on the emission properties of ZnO films prepared on Si(100) by RF magnetron sputtering, J. Phys. D Appl. Phys. 36, 2017−2020 **(2003).**

[27] M. Krunks, T. Dedova, E. Karber, V. Mikli, I. Oja Acik, M. Grossnerg, A. Mere, Growth and electrical properties of ZnO nanorod arrays prepared by chemical spray pyrolysis, Physica B 404, 4422-4425 **(2009).**

[28] J. Lang, J. Wang, Q. Zhang, X. Songsong, Q. Han, Y. Zhang, Hongju. Zhai, J. Cao, Y. Yan, J. Yang, Rapid synthesis and photoluminescence properties of Eu-doped ZnO nanoneedles *via* facile hydrothermal method, Chem. Res. Chin. Univ. 30, 538-542 **(2014).**

[29] L.L. Yang, Q.X. Zhao, M. Willander, X.J. Liu, M. Fahlman, J.H. Yang, Origin of the surface recombination centers in ZnO nanorods arrays by X-ray photoelectron spectroscopy, Appl. Surf. Sci. 256, 3592-3597 **(2010).**

[30] S. Anandan, A. Vinu, K. Lovely, N. Gokulakrishnan, P. Srinivasu, T. Mori, V. Murugesan, V. Sivamurugan and K. Ariga, Photocatalytic activity of La-doped ZnO for the

degradation of monocrotophos in aqueous suspension, J. Mol. Catal. A: Chem. 266, 149–157 **(2007).**

[31] A. Godlyn Abraham, A. Manikandan, E. Manikandan, S. K. Jaganathan, A. Baykal, P. Sri Renganathan, Enhanced Opto-Magneto Properties of $Ni_xMg_{1-x}Fe_2O_4$ ($0.0 \leq x \leq 1.0$) Ferrites Nano-Catalysts, Journal of Nanoelectronics and Optoelectronics 12, 1326–1333 **(2017).**

[32] A. Silambarasu, A. Manikandan, K. Balakrishnan, Room temperature superparamagnetism and enhanced photocatalytic activity of magnetically reusable spinel $ZnFe_2O_4$ nano-catalysts, Journal of Superconductivity and Novel Magnetism, 30, 2631–2640 **(2017).**

[33] A. Godlyn Abraham, A. Manikandan, E. Manikandan, S. Vadivel, S. K. Jaganathan, A. Baykal, P. Sri Renganathan, Enhanced magneto-optical and photo-catalytic properties of transition metal cobalt (Co^{2+} ions) doped spinel $MgFe_2O_4$ ferrite nanocomposites, Journal of Magnetism and Magnetic Materials, 452, 380-388 **(2018).**

[34] R. Bomila, S. Srinivasan, S. Gunasekaran, A. Manikandan, Enhanced photocatalytic degradation of methylene blue dye, opto-magnetic and antibacterial behaviour of pure and La-doped ZnO nanoparticles, J. Supercond. Nov. Magn. 31, 855–864 **(2018).**

[35] K. Chitra, K. Reena, A. Manikandan, S. Arul Antony, Antibacterial studies and effect of poloxamer on gold nanoparticles by Zingiber officinale extracted green synthesis, J. Nanosci. Nanotech. 15, 4984-4991 **(2015).**

[36] K. Chitra, A. Manikandan, S. Moortheswaran, K. Reena, S. Arul Antony, Zingiber officinale extracted green synthesis of copper nanoparticles: Structural, morphological and antibacterial studies, Adv. Sci., Eng. Med. 7, 710-716 **(2015).**

[37] K. Chitra, A. Manikandan, S. Arul Antony, Effect of poloxamer on Zingiber officinale extracted green synthesis and antibacterial studies of silver nanoparticles, J. Nanosci. Nanotech. 16, 758-764 **(2016).**

[38] A. T. Ravichandran, J. Srinivas, R. Karthick, A. Manikandan, A. Baykal, Facile combustion synthesis, structural, morphological, optical and antibacterial studies of $Bi_{1-x}Al_xFeO_3$ ($0.0 \leq x \leq 0.15$) nanoparticles, Ceramics International, 44, 13247-13252 **(2018).**

List of Figures

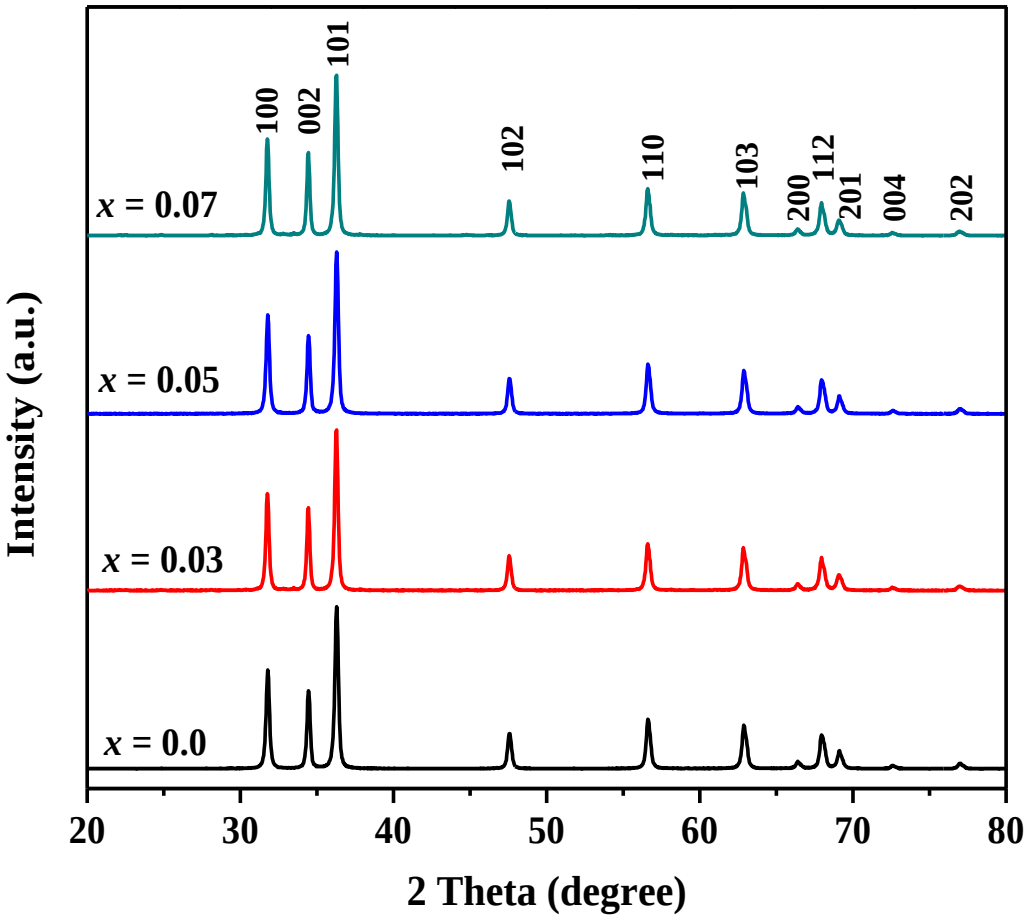

Figure 1. X-ray powder patterns $Ce_xZn_{1-x}O$ ($0.0 \leq x \leq 0.07$) NPs

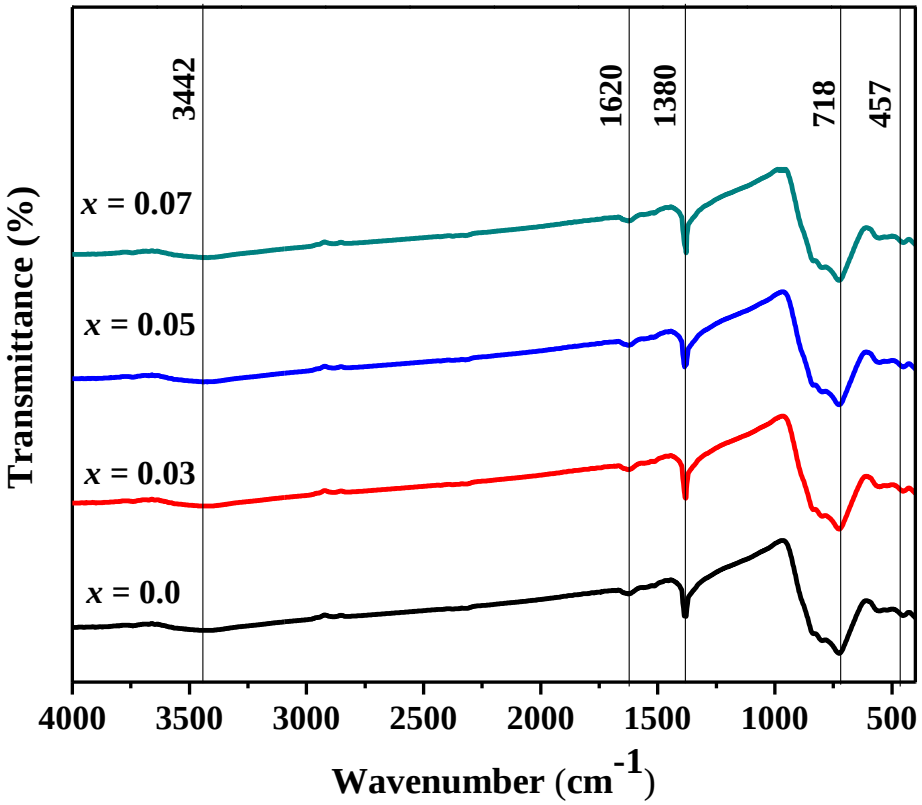

Figure 2. FT-IR spectra of $Ce_xZn_{1-x}O$ ($0.0 \leq x \leq 0.07$) NPs

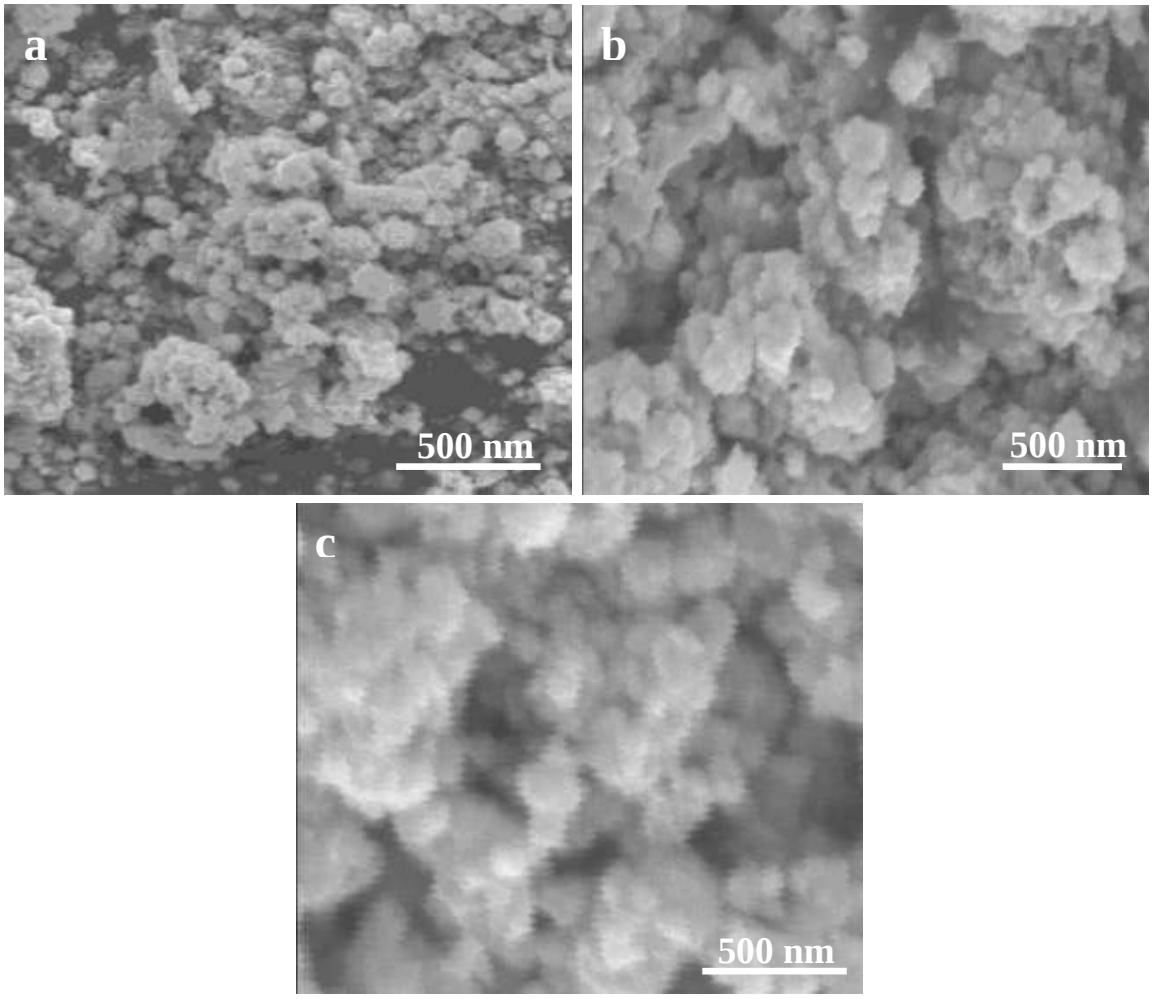

Figure 3. HR-SEM images of $Ce_xZn_{1-x}O$ (**(a)** x = 0.0, **(b)** x = 0.05 and **(c)** x = 0.07) NPs

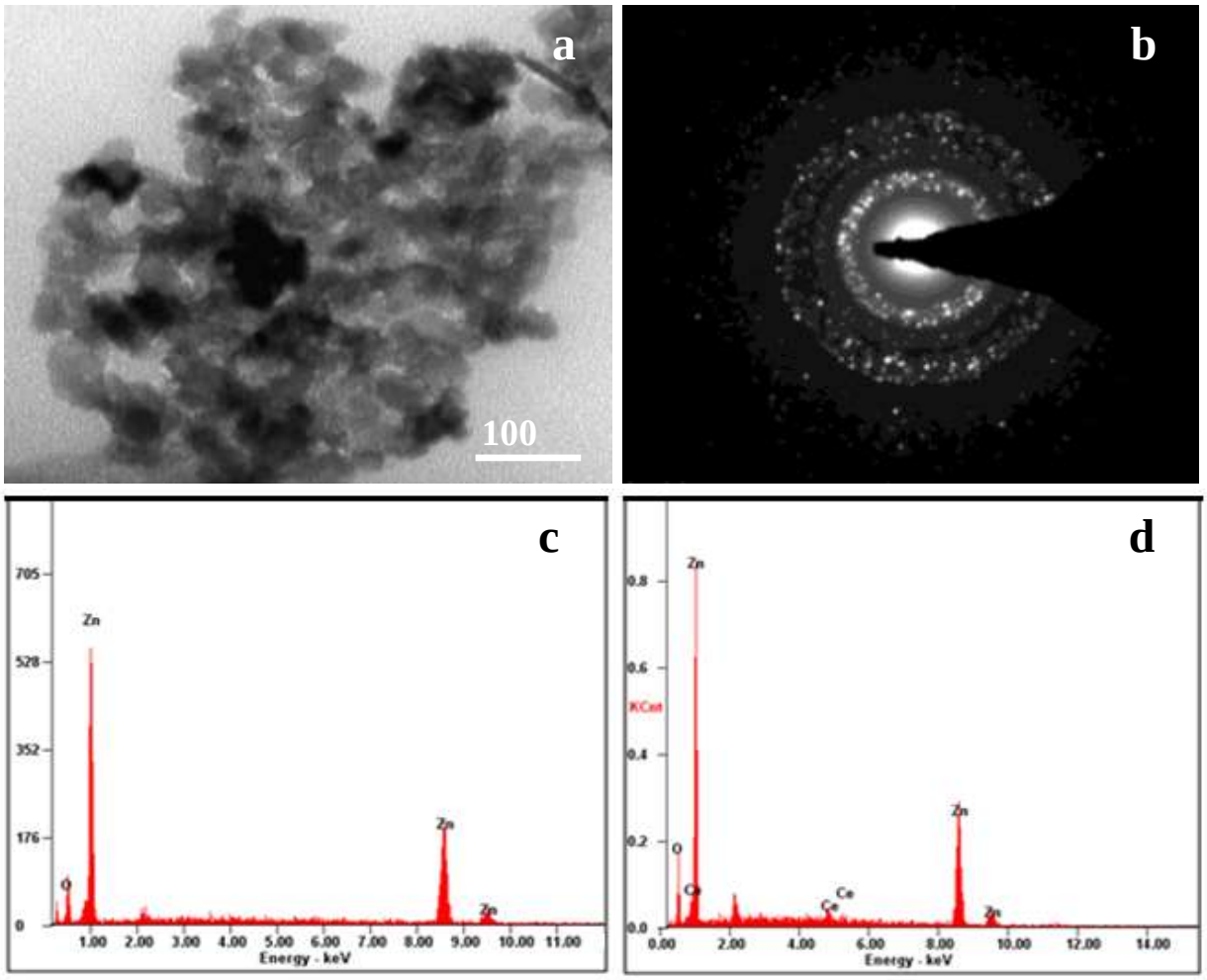

Figure 4. (a) HR-TEM image (x = 0.05M), **(b)** corresponding SAED pattern (x = 0.05) and **(c, d)** EDX spectrum (x = 0.0, x = 0.05) of $Ce_xZn_{1-x}O$ NPs.

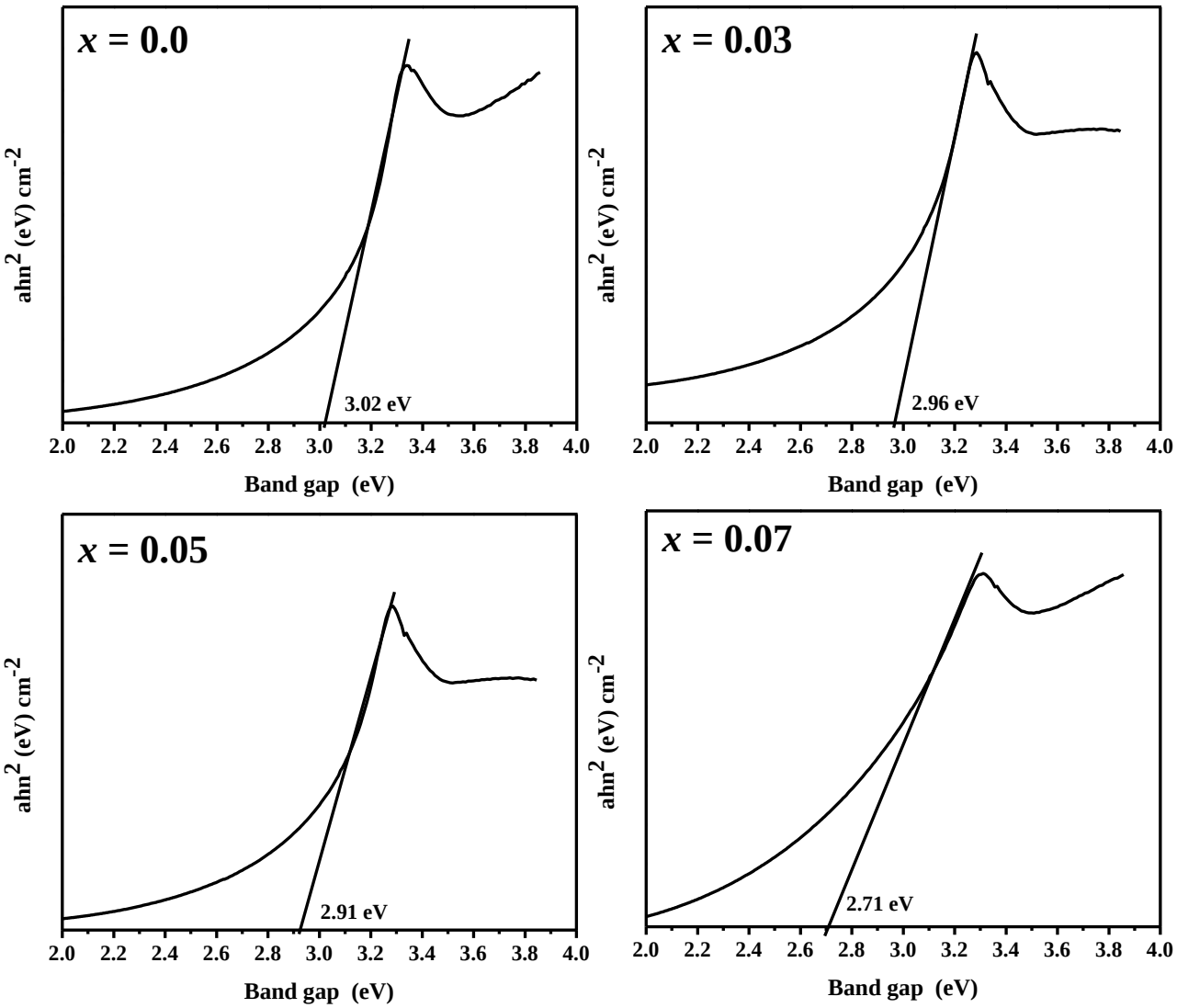

Figure 5. Tauc plots drawn $(\alpha h\nu)^2$ versus photon energy ($h\nu$) of $Ce_xZn_{1-x}O$ ($0.0 \leq x \leq 0.07$) NPs

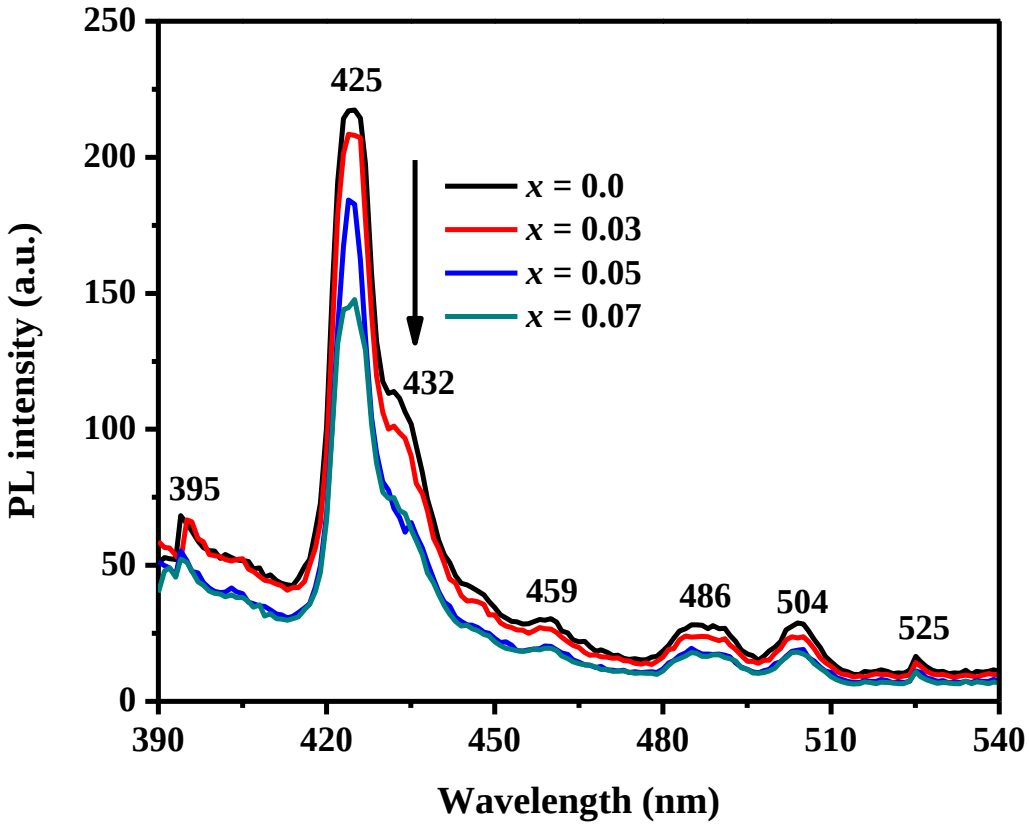

Figure 6. PL spectrum of $Ce_xZn_{1-x}O$ ($0.0 \leq x \leq 0.07$) NPs

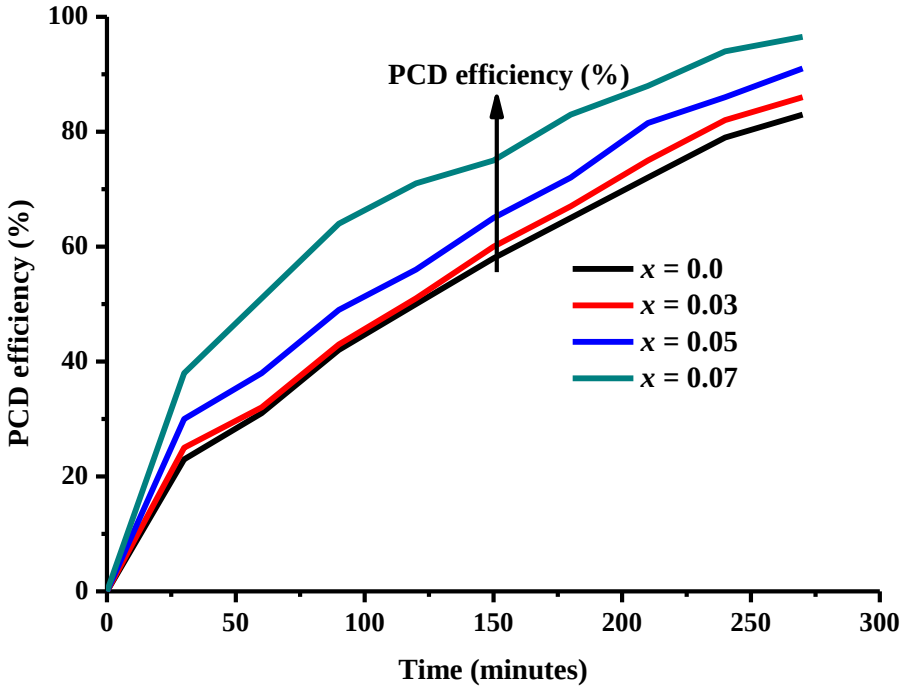

Figure 7. PCD efficiency of $Ce_xZn_{1-x}O$ ($0.0 \leq x \leq 0.07$) NPs

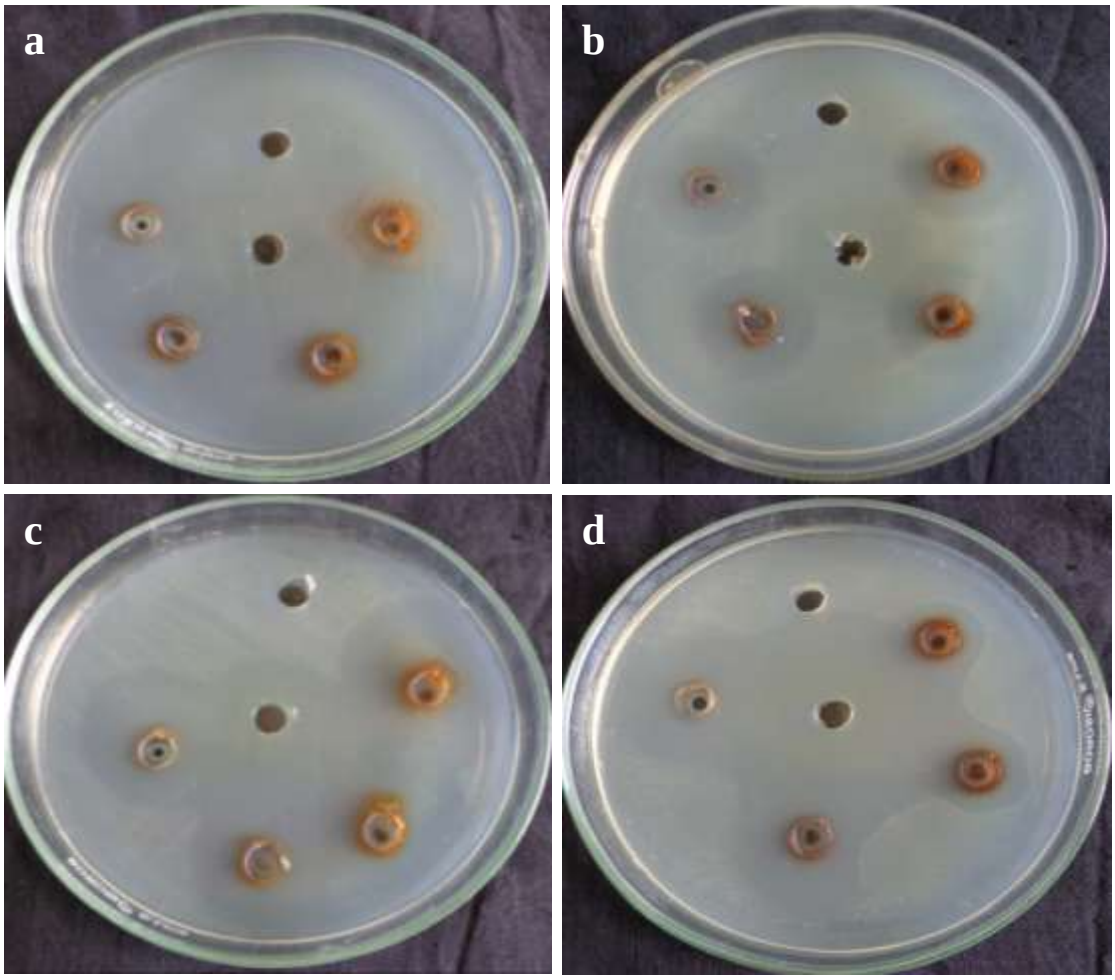

Figure 8. Antibacterial activity of pure and Ce doped ZnO nanoparticles against **(a)** P. mirabilis, **(b)** S. typhi, **(c)** S. aureus and (d) B. subtilis

Table 1. Structural parameters (Lattice constant and Crystallite size) and energy band gap of $Ce_xZn_{1-x}O$ ($0.0 \leq x \leq 0.07$) NPs.

x	Lattice parameter (Å)			D	V	E_g
	a	c	c/a	(nm)	$(Å)^3$	(eV)
0.0	3.251	5.211	1.603	15.64	53.92	3.02
0.03	3.258	5.218	1.601	14.55	52.56	2.96
0.05	3.265	5.225	1.600	13.46	53.12	2.91
0.07	3.274	5.234	1.598	12.33	52.28	2.71

Table 2. Antibacterial activities of $Ce_xZn_{1-x}O$ ($0.0 \leq x \leq 0.07$) NPs for against human pathogens

Antibacterial activities of samples were determined as zone of inhibition (in mm)				
Samples	***P. mirabilis***	***S .typhi***	***S. aureus***	***B. subtilis***
Ampicillin (C)	24	19	12	11
$x = 0$	8	7	4	7
$x = 0.03$	7	11	6	4
$x = 0.05$	19	17	9	6
$x = 0.07$	21	9	5	8